Molecular Engineering of Conjugated Polymer Cathodes via One-Pot Preparation for High-Rate and Ultra-Stable Aqueous/Seawater Zn-Ion Batteries under Harsh Conditions

Quanwei Ma,‡[a] Cheng Ji,‡[a] Zeyu Wang,[b] Rui Wang,[a] Longhai Zhang,[a] Hongbao Li,[a] Ying Xu,[c] Qianyu Zhang,[d] Dongliang Chao,*[b] and Chaofeng Zhang*[a]

[a.] Institutes of Physical Science and Information Technology, Leibniz International Joint Research Centre of Materials Sciences of Anhui Province, Key Laboratory of Environment-Friendly Polymeric Materials of Anhui Province, Anhui University, Hefei 230601, China.

[b.] Laboratory of Advanced Materials, Aqueous Battery Center, Shanghai Key Laboratory of Molecular Catalysis and Innovative Materials, Collaborative Innovation Center of Chemistry for Energy Materials, Shanghai Wusong Laboratory of Materials Science, State Key Laboratory of Porous Materials for Separation and Conversion, College of Smart Materials and Future Energy, Fudan University, Shanghai 200433, China;

[c.] School of Materials Science and Engineering, Anhui University, Hefei 230601, China.

[d.] College of Materials Science and Engineering, Sichuan University, Chengdu 610064, China.

‡ These authors contribute to this work equally.

* Corresponding author：E-mail: chaod@fudan.edu.cn; cfz@ahu.edu.cn

Experimental section

Synthesis of PMPZ

In a glove box, 1 mmol of mellitic trianhydride, 1.5 mmol of phenazine, and 5 mmol of anhydrous zinc chloride were thoroughly mixed and ground. The mixture was subsequently transferred to a glass tube, which was evacuated, backfilled with nitrogen, and flame-sealed. After heating at 300 °C for 24 h, the sealed tube was cooled to room temperature, yielding a black crude product. Then, the product was ground and then cautiously added to dilute hydrochloric acid (100 mL) in an ice-water bath. After filtration, the solid was washed sequentially with water, DMF, and ethanol, and then dried under vacuum at 80 °C for 12 hours. Finally, 324 mg of the black solid product was obtained, with a yield of approximately 58%.

Material characterization

The chemical composition of the samples was characterized using Fourier transform infrared spectrometry (FT-IR, Thermo Scientific Nicolet iS5), X-ray photoelectron spectroscopy (XPS, ESCALAB 250 Xi), X-ray diffraction (XRD, D2 PHASER with Cu Kα radiation), and solid-state nuclear magnetic resonance (SSNMR, ^{13}C). Thermal stability was evaluated by thermogravimetric analysis (TGA, STA449 F5) in air from 30 to 800 ℃.

Optical Energy Gap

The optical energy gaps (*E*g, eV) of the PMPZ cathodes can be determined by the ultraviolet-visible (UV-Vis) spectroscopy, as followed formula:

$$\alpha \propto \frac{(hv-E_g)^{1/2}}{hv}$$

$$hv=1280/\lambda$$

where α is the absorption coefficient, hv represents the photon energy, and λ denotes the wavelength.

Theoretical Specific Capacity

The theoretical specific capacity of the PMPZ cathode material can be obtained by using the following equation:

$$Q_{spec}=\frac{n\cdot F}{3.6\cdot M_w}=\frac{26801\cdot n}{M_w}$$

where M_w is the relative molecular weight of the repeating unit in PMPZ skeleton (336 g mol^{-1}), and n stands for the number of electrons transferred per unit (a 6-electron reaction). As a result, the theoretical capacity of the PMPZ cathode is calculated to be 478.6 mA h g^{-1}.

Electrochemical tests

The cathodes were fabricated by coating a slurry of PMPZ, conductive carbon (Ketjen

black), and PVDF (5:4:1 by mass) in NMP onto Ti foil, followed by vacuum drying at 80 °C for 12 h (Areal mass loading of active material on current collector is 0.8 mg cm^{-2}). CR2032-type coin cells were configured with a Zn foil anode (Thickness of 50 μm), 3 M $Zn(ClO_4)_2$ electrolyte (50 μL), and a glass fiber separator (Thickness of 420 μm) to evaluate the electrochemical performance of AZIBs. All assembly was performed in ambient air at room temperature. Electrochemical performance for PMPZ was tested within a voltage range from 0.2 to 1.6 V on NEWARE. The electrochemical behavior of PMPZ was characterized using Cyclic voltammetry (CV) and electrochemical impedance spectroscopy (EIS) employed a CHI 760C workstation, with a voltage range from 0.2 to 1.6 V and the latter in a frequency range of 100 kHz to 0.01 Hz. Additionally, the galvanostatic intermittent titration technique (GITT) was conducted on a NEWARE system within the 0.2-1.6 V window.

Zn//PMPZ pouch cell: The PMPZ cathode is fabricated using a dry electrode process. In this method, the active material, conductive carbon (Ketjen black), and PTFE are blended into a homogeneous slurry, which is then rolled onto a titanium mesh current collector (4 cm × 5 cm, the active material loading is 5 mg cm^{-2}). The pouch cell configuration consists of a Zn foil anode (10 μm in thickness), 500 μL of 3 M $Zn(ClO_4)_2$ electrolyte, and a glass fiber separator (420 μm in thickness), with an N/P ratio (capacity ratio of the negative electrode to the positive electrode) of 5.8:1.

***Operando Synchrotron FT-IR Measurements*:** The reaction mechanism was characterized by *Operando* synchrotron FT-IR spectroscopy. A Zn//PMPZ battery in a dedicated cell (Beijing Scistar Technology Co. Ltd) was cycled at 0.1 A g^{-1} (NEWARE tester). The synchrotron FT-IR data were simultaneously collected at the BL01B beamline.

In situ EQCM-D measurements: The measurement of mass changes during electrochemical reaction was conducted using an in-situ electrochemical quartz crystal microbalance with dissipation monitoring (EQCM-D) and a Biolin Scientific Qsense Analyzer. This technique focuses on obtaining the ratio of mass changes to charge transfer (Δm/Δq), which is calculated by the following Faraday's equation.

$$\frac{\Delta m}{\Delta q} = \frac{M}{n F}$$

where Δm stands for the mass change (g), Δq stands for the charge transfer (C), F is the Faraday constant (96485 C mol^{-1}), M is the relative atomic mass, and n is the electron transfer number.

The theoretical value of Zn^{2+} to react with PMPZ is calculated based on the following equation:

$$\frac{\Delta m}{\Delta q} = \frac{M}{n F} = \frac{65}{2\times 96485}\,mg/C = 0.337 mg/C$$

The theoretical value of H^+ to react with PMPZ is calculated based on the following

equation:

$$\frac{\Delta m}{\Delta q} = \frac{M}{n\,F} = \frac{1}{1\times 96485}\,mg/C = 0.01mg/C$$

Calculation

All calculations were performed using DFT theoretical calculations on B3LYP combined with the 6-31G(d) basis set in Gaussian16.[1, 2] Additionally, we incorporated the Grimme D3(BJ) dispersion correction to further refine our calculation, and further analysis was performed using the software Multiwfn 3.8 and VMD 1.9.3. The energies of the highest occupied molecular orbital (HOMO) and the lowest unoccupied molecular orbital (LUMO), as well as the harmonic oscillator model of aromaticity (HOMA) index, were obtained from these simulations.

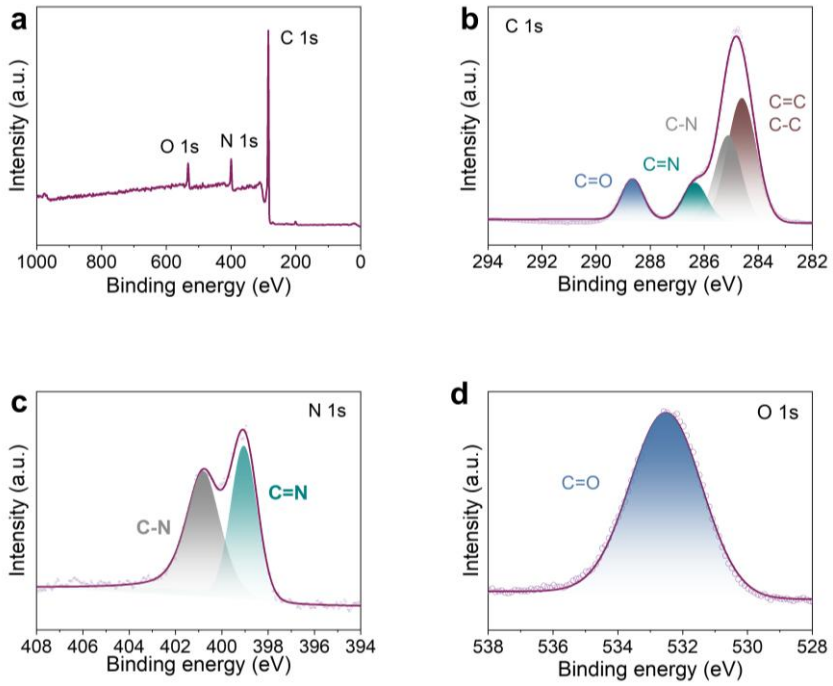

Figure S1. (a) The XPS survey spectrum of PMPZ. (b) The XPS spectrum of C 1s of PMPZ. High resolution XPS spectra of (c) N 1s and (d) O 1s of PMPZ.

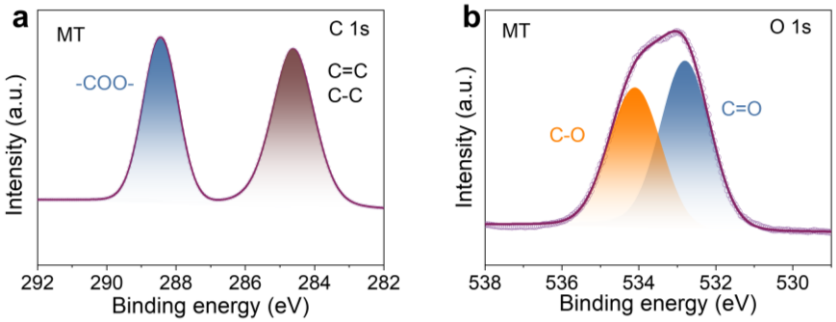

Figure S2. High resolution XPS spectra of (a) C 1s and (b) O 1s for MT.

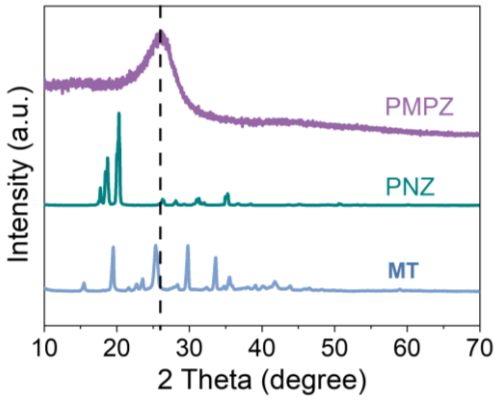

Figure S3. XRD patterns of MT, PNZ, and PMPZ.

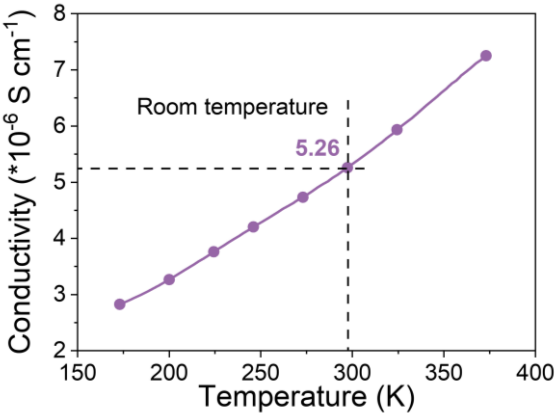

Figure S4. The electronic conductivity vs. temperature curves for PMPZ.

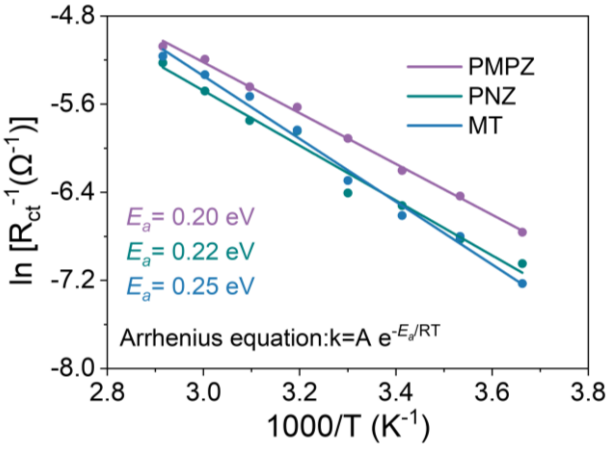

Figure S5. The Arrhenius plots of ln(Rct^{-1}) vs. 1000/T.

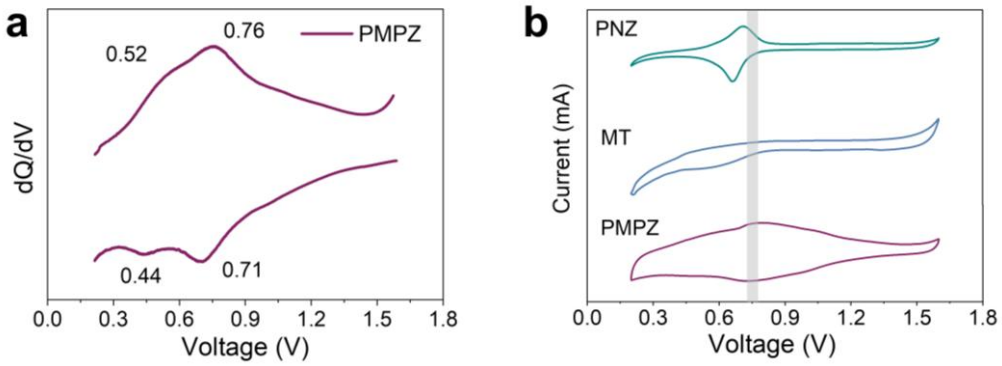

Figure S6. (a) The dQ/dV curve of PMPZ. (b) CV curves of PNZ, MT, and PMPZ at 0.1 mV s^{-1}.

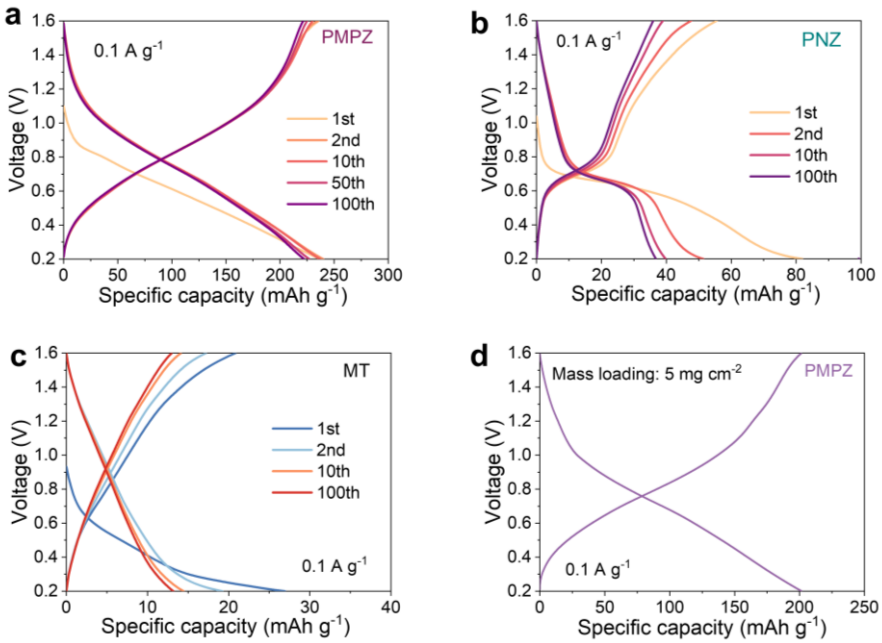

Figure S7. (a) Charge/discharge curves of PMPZ at 0.1 A g^{-1}. (b) Charge/discharge curves of PNZ at 0.1 A g^{-1}. (c) Charge/discharge curves of MT at 0.1 A g^{-1}. (d) Charge/discharge curves of PMPZ with high mass-loading of 5 mg cm^{-2} at 0.1 A g^{-1}.

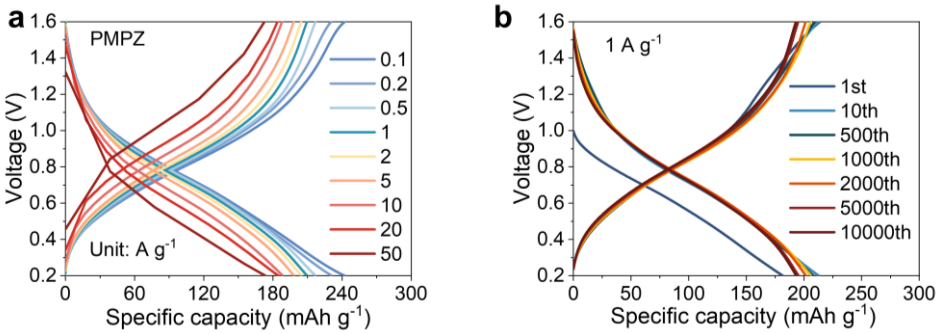

Figure S8. (a) Charge/discharge curves of PMPZ at different current densities. (b) Charge/discharge curves of PMPZ at 1 A g^{-1}.

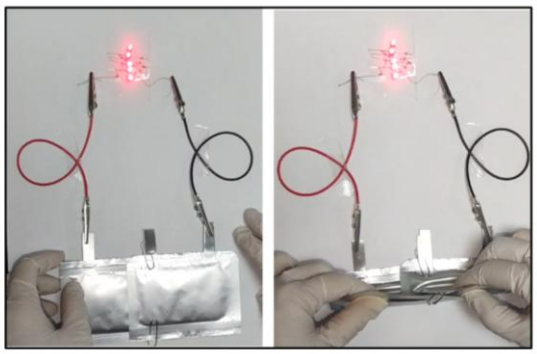

Figure S9. The practicality evaluation of Zn//PMPZ pouch cells by powering LED lights.

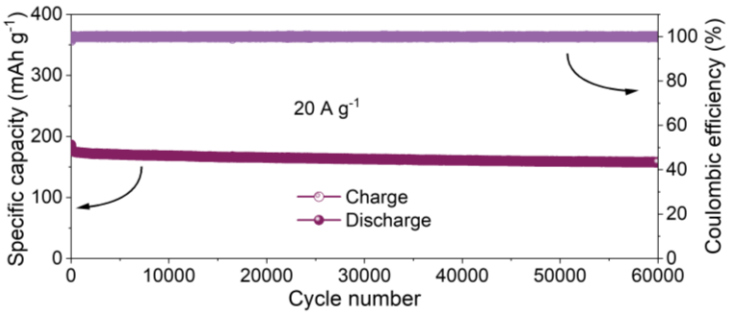

Figure S10. Long-term cycling stability of PMPZ at 20 A g^{-1}.

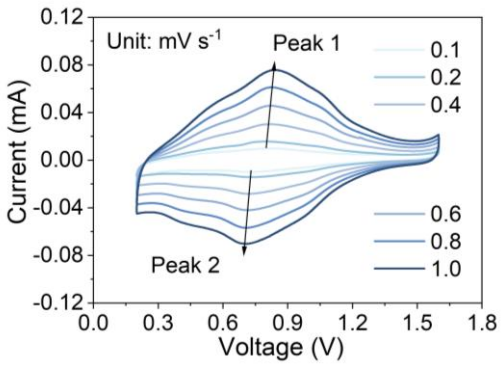

Figure S11. CV curves of PMPZ at different scan rates.

The electrochemical behavior was evaluated through calculating the b-values, which based on peak current (i) and scan rate (v), as portrayed in the formula:[3-5]

$$i=av^b$$

$$\log(i)=\log(a)+b\log(v)$$

The constants a and b are adjustable parameters, with the b-value specifically characterizing the charge storage process. b = 0.5 represents diffusion-controlled kinetics, while b = 1.0 indicates ideal pseudocapacitive behavior.

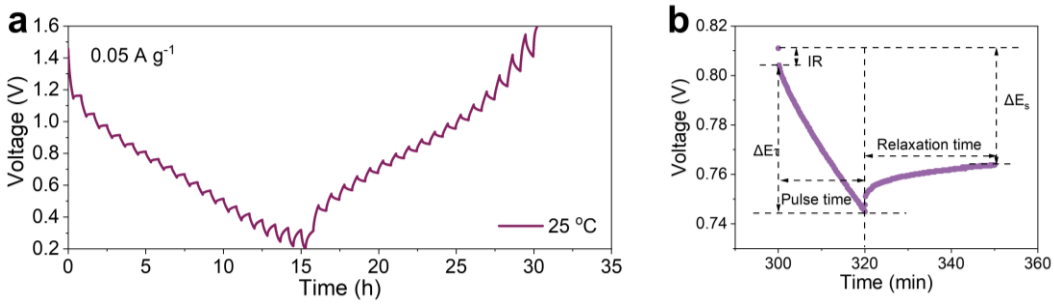

Figure S12. (a) GITT curve of PMPZ at 0.05 A g^{-1} under 25 °C. (b) Schematic diagram of calculating the diffusion coefficient of Zn^{2+} via GITT measurement.

In addition, the electrochemical kinetics of PMPZ were further evaluated via GITT (**Figure S12**). The corresponding Zn^{2+} diffusion coefficients ($D_{Zn^{2+}}$) were calculated from GITT data using equation (3).[6, 7]

$$D = \left(\frac{4L^2}{\pi\tau}\right) \times \left(\frac{\Delta E_s}{\Delta E_\tau}\right)^2$$

Where L denotes diffusion length (20 μm), τ indicates the relaxation time, ΔE_τ represents the voltage change, and ΔE_s represents the equilibrium potential change.

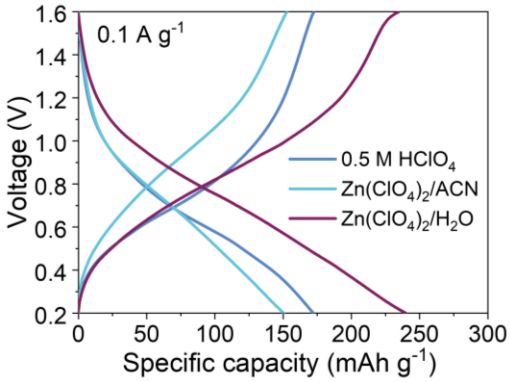

Figure S13. Charge/discharge profiles of PMPZ in different electrolytes.

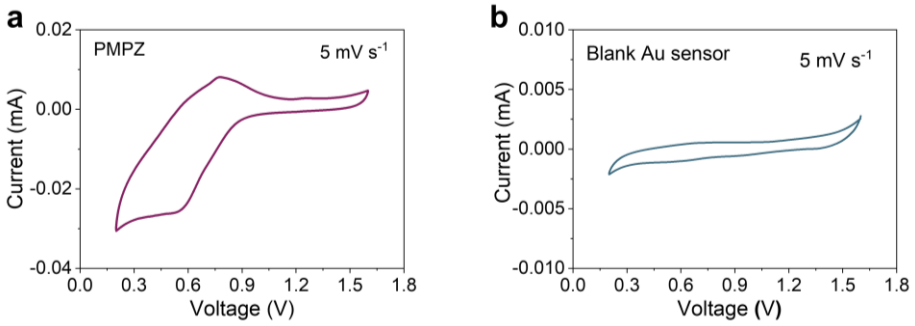

Figure S14. (a) CV curves of PMPZ at 5 mV s^{-1}. (b) CV curves of blank Au sensor at 5 mV s^{-1}.

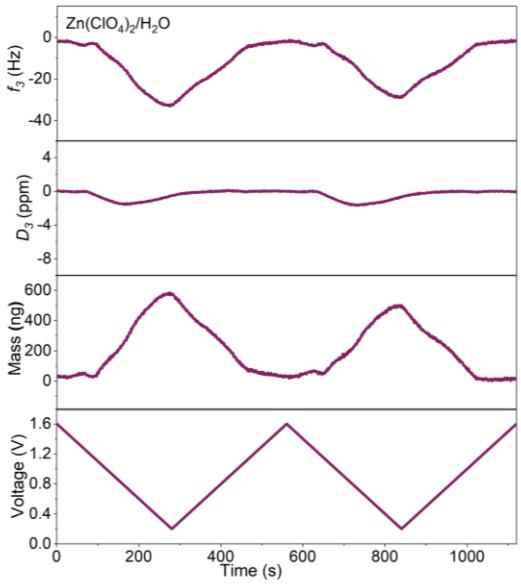

Figure S15. *Operando* EQCM-D response (f_3 and D_3) and mass change of PMPZ at 5 mV s^{-1}.

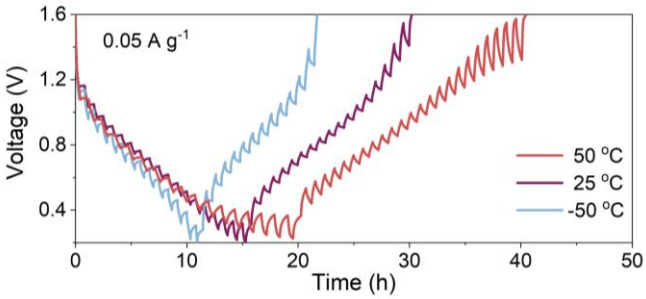

Figure S16. GITT curves of PMPZ at 0.05 A g^{-1} under 50, 25, and −50 °C.

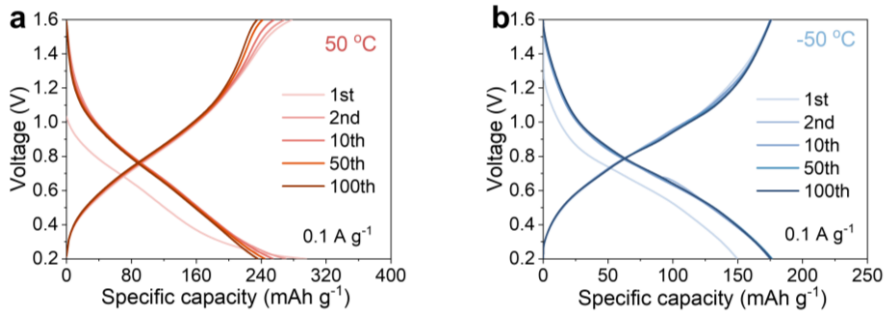

Figure S17. Charge/discharge curves of PMPZ at 0.1 A g^{-1} under (a) 50 °C and (b) −50 °C.

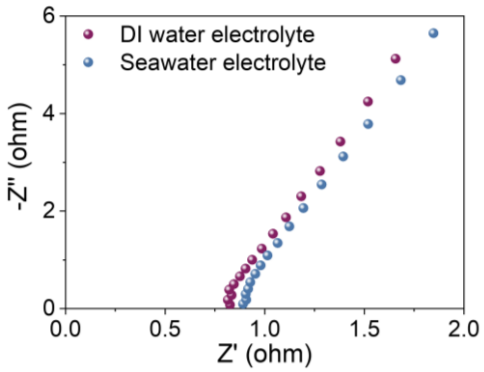

Figure S18. EIS plots of the steel//steel symmetric cell with DI water-based and seawater-based electrolytes.

Table S1. Comparison of specific capacity and cycling performance for reported organic materials for ZIBs.

Organic Cathode	Electrolyte	Capacity (mAh g^{-1})	Cycling performance Capacity retention (%)	Ref.
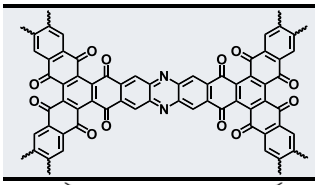	3M $Zn(ClO_4)_2$	240@0.1 A g^{-1} 179@50 A g^{-1}	90, 60000 cycles, 20 A g^{-1}	This work
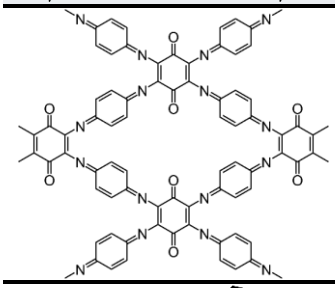	1 M $ZnSO_4$	208@0.1 A g^{-1} 136@2 A g^{-1}	87, 1000 cycles, 1 A g^{-1}	8
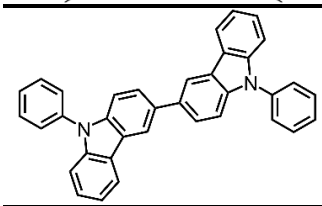	20 M LiTFSI + 1 M $Zn(TFSI)_2$	100@0.05A g^{-1} 76@0.5 A g^{-1}	95, 1000 cycles, 10 A g^{-1}	9
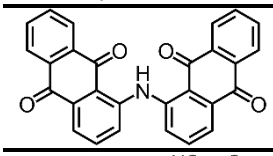	3 M $Zn(OTf)_2$	141@0.025A g^{-1}	96, 5000 cycles 2 A g^{-1}	10
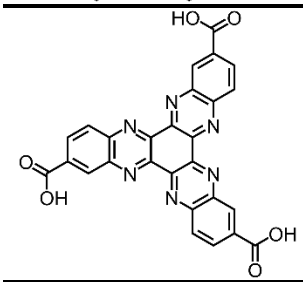	1 M $Zn(OTf)_2$	226@0.05 A g^{-1} 145@25 A g^{-1}	84.07, 10000 cycles 25 A g^{-1}	11
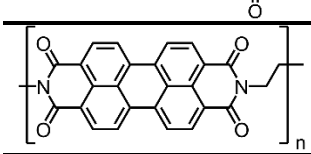	2 M $ZnSO_4$	118@0.05A g^{-1} 95@5 A g^{-1}	70.5, 1500 cycles, 1 A g^{-1}	12
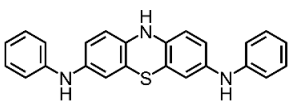	2 M $ZnSO_4$	145.6@0.1 A g^{-1} 52@5 A g^{-1}	82.5, 4000 cycles, 1 A g^{-1}	13
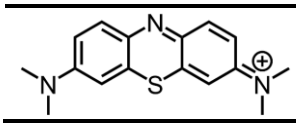	3 M $Zn(OTF)_2$	142@0.167 A g^{-1} 58@83.5 A g^{-1}	86, 20000 cycles, 16.7 A g^{-1}	14

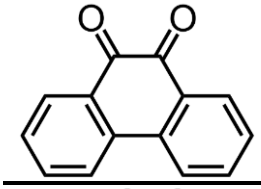	2 M $ZnSO_4$	150@0.1 A g^{-1} 107.8@5 A g^{-1}	96.3, 36000 cycles, 5 A g^{-1}	15
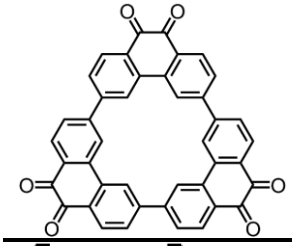	3 M $Zn(OTF)_2$	210@0.15 A g^{-1}	99, 500 cycles, 0.15 A g^{-1}	16
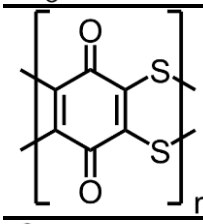	4 M $Zn(OTF)_2$	205@0.05 A g^{-1} 176@10 A g^{-1}	80, 10000 cycles, 20 A g^{-1}	17
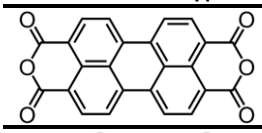	2 M $ZnCl_2$	122.9@0.2 A g^{-1} 76.9@32 A g^{-1}	68.2, 1000 cycles, 8 A g^{-1}	18
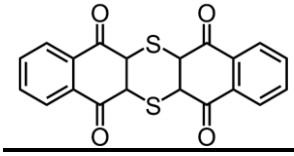	2 M $ZnSO_4$	210.9@0.05 A g^{-1} 97@2 A g^{-1}	83.8, 23000 cycles, 2 A g^{-1}	19
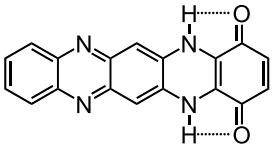	2M $Zn(ClO_4)_2$	204@0.2 A g^{-1} 114.2@30 A g^{-1}	85, 2000 cycles, 2 A g^{-1}	20
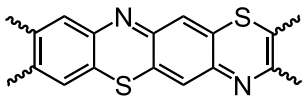	1 M $Zn(OTF)_2$	120.5@1 A g^{-1} 60.7@20 A g^{-1}	87, 7000 cycles, 5 A g^{-1}	21
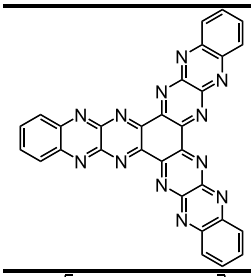	2 M $ZnSO_4$	198.47@0.2 A g^{-1} 121.4@5 A g^{-1}	94, 1000 cycles, 2 A g^{-1}	22
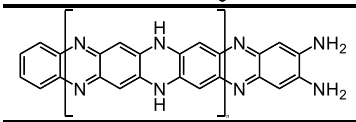	2 M $ZnSO_4$	236.2@0.2 A g^{-1} 88.36@30 A g^{-1}	79, 139000 cycles, 10 A g^{-1}	23
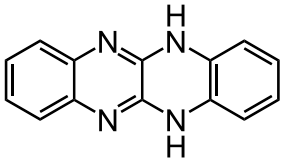	3 M $Zn(ClO_4)_2$	200.3@0.1 A g^{-1} 88.5@10 A g^{-1}	73, 5000 cycles, 5 A g^{-1}	24
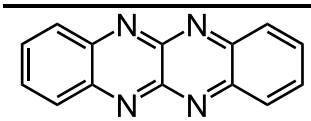	3 M $Zn(OTF)_2$	202@0.115 A g^{-1} 121@4.6 A g^{-1}	71, 47500 cycles, 5 A g^{-1}	25

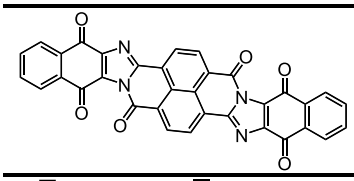	3 M $Zn(ClO_4)_2$	235@0.2 A g^{-1} 189@10 A g^{-1}	89, 50000 cycles, 10 A g^{-1}	26
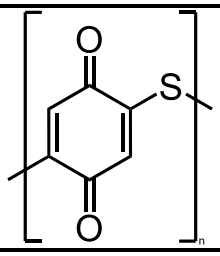	1 M $Zn(OTF)_2$/DMF	200@0.1 A g^{-1} 100@10 A g^{-1}	66, 10000 cycles, 2 A g^{-1}	27

Reference

1. M. Frisch, G. Trucks, H. Schlegel, G. Scuseria, M. Robb, J. Cheeseman, G. Scalmani, V. Barone, G. Petersson and H. Nakatsuji, *Gaussian Inc., Wallingford CT,*, 2016.
2. R. G. Parr, Yang, W. Density-Functional Theory of Atoms and Molecules. Oxford University Press (1989).
3. Y. Zhang, Q. Huang, Z. Song, L. Miao, Y. Lv, L. Gan and M. Liu, *Adv. Funct. Mater.*, 2024, **35**, 2416415.
4. Z. Yang, P. Meng, M. Jiang, X. Zhang, J. Zhang and C. Fu, *Angew. Chem. Int. Ed.*, 2024, **63**, e202403424.
5. T. Ji, X. Liu, T. Zhang, Y. Shi, D. Sheng, H. Yin, Z. X. Shen and D. Chao, *Adv. Energy Mater.*, 2024, **14**, 2401908.
6. J. Ning, X. Zhang, D. Xie, Q. He, J. Hu, J. Tang, R. Li, H. Meng and K. X. Yao, *Angew. Chem. Int. Ed.*, 2024, **63**, e202319796.
7. L. Zhang, J. Liu, Y. Zhai, S. Zhang, W. Wang, G. Li, L. Sun, H. Li, S. Qi, S. Chen, R. Wang, Q. Ma, J. Just and C. Zhang, *Adv. Mater.*, 2024, **36**, 2313835.
8. Z. Lin, L. Lin, J. Zhu, W. Wu, X. Yang and X. Sun, *ACS Appl. Mater. Interfaces*, 2022, **14**, 38689-38695.
9. U. Mittal, F. Colasuonno, A. Rawal, M. Lessio and D. Kundu, *Energy Storage Mater.*, 2022, **46**, 129-137.
10. X. Geng, Y. Jiang, H. Ma, H. Zhang, J. Liu, Z. Zhang, C. Peng, J. Zhang, Q. Zhao and N. Zhu, *ACS Appl. Mater. Interfaces*, 2022, **14**, 49746-49754.
11. J. Li, L. Huang, H. Lv, J. Wang, G. Wang, L. Chen, Y. Liu, W. Guo, F. Yu and T. Gu, *ACS Appl. Mater. Interfaces*, 2022, **14**, 38844-38853.
12. B. Jiang, T. Huang, P. Yang, X. Xi, Y. Su, R. Liu and D. Wu, *Journal of Colloid and Interface Science*, 2021, **598**, 36-44.
13. N. Wang, Z. Guo, Z. Ni, J. Xu, X. Qiu, J. Ma, P. Wei and Y. Wang, *Angew. Chem. Int. Ed.*, 2021, **60**, 20826-20832.
14. M. Tang, Q. Zhu, P. Hu, L. Jiang, R. Liu, J. Wang, L. Cheng, X. Zhang, W.

Chen and H. Wang, *Adv. Funct. Mater.*, 2021, **31**, 2102011.

15. B. Yang, Y. Ma, D. Bin, H. Lu and Y. Xia, *ACS Appl. Mater. Interfaces*, 2021, **13**, 58818-58826.
16. K. W. Nam, H. Kim, Y. Beldjoudi, T.-w. Kwon, D. J. Kim and J. F. Stoddart, *J. Am. Chem. Soc.*, 2020, **142**, 2541-2548.
17. J. Xie, F. Yu, J. Zhao, W. Guo, H.-L. Zhang, G. Cui and Q. Zhang, *Energy Storage Mater.*, 2020, **33**, 283-289.
18. H. Zhang, Y. Fang, F. Yang, X. Liu and X. Lu, *Energy Environ. Sci.*, 2020, **13**, 2515-2523.
19. Y. Wang, C. Wang, Z. Ni, Y. Gu, B. Wang, Z. Guo, Z. Wang, D. Bin, J. Ma and Y. Wang, *Adv. Mater.*, 2020, **32**, 2000338.
20. X. Liu, J. Tang, D. Bin, Y. Wang, C. Li, L. Su, Y. Shen, W. Hu, Z. Hu, W. Zhuang, B. Yang, H. Lu and Y. Wang, *Energy Storage Mater.*, 2025, **81**.
21. L. Zhao, Y. Jia, Y. Wu, T. Gu, X. Zhou, X. Wang, L. Zhong, S. Zhan, H. Lv, C. Zhi and J. Liu, *Angew. Chem. Int. Ed.*, 2025, **64**, e202425082.
22. R. Wang, Y. Zhang, C. Ma, X. Wang, M. Cai, H. Du, Z. Yang, D. Chao and Y. Wang, *Adv. Funct. Mater.*, 2025, **35**, 2505318.
23. S. Niu, L. Zhao, Y. Wang, Q. Luo, H. Xue, N. Ju, Y. Wang, L. Zhu, B. Xu, L. Sun, Y. Zhao, H. Liu, J. Bouwer, Y. X. Wang, S. X. Dou, H. K. Liu, G. W. Xu, H. b. Sun and W. H. Lai, *Angew. Chem. Int. Ed.*, 2025, **64**.
24. Y. Zhang, M. Li, Z. Li, Y. Lu, H. Li, J. Liang, X. Hu, L. Zhang, K. Ding, Q. Xu, H. Liu and Y. Wang, *Angew. Chem. Int. Ed.*, 2024, **63**, e202410342.
25. D. Du, J. Zhou, Z. Yin, G. Feng, W. Ji, H. Huang and S. Pang, *Adv. Energy Mater.*, 2024, **14**, 2400580.
26. P. Xiong, B. Liu, S. Zhang, G. Li, X. Zhang, R. Wang, H. Li, G. Feng, L. Zhang and C. Zhang, *Adv. Funct. Mater.*, 2026, DOI: 10.1002/adfm.74641.
27. X. Yu, K. Zhou, C. Liu, J. Li, J. Ma, L. Yan, Z. Guo and Y. Wang, *Angew. Chem. Int. Ed.*, 2025, **64**.